

chromatizing and manipulating x-ray beams at fourth-generation x-ray sources. Given this, examining the fundamental physics of perfect-crystal diffraction (i.e., dynamical diffraction theory) in the regime of ultrashort (femtosecond) pulses is worthwhile. In this regime, the pulse lengths are comparable to or shorter than the extinction length scales of the crystal reflection. We have developed computer programs to calculate the diffraction properties under ultrashort pulses, initially without consideration of damage due to the high peak fields. Initial work consisted of computation of the Green's functions corresponding to crystal-reflection responses to incident δ -function electromagnetic impulses in Bragg and Laue geometries, for both reflected and transmitted beams. In addition to demonstrating quantitatively how crystal reflections respond to impulses, these

simulations pointed out the effect of delayed echos from back-face diffraction in thin Bragg crystals. (A similar effect exists for Laue crystals.) The studies were taken further to examine the modification of a self-amplified spontaneous emission (SASE) x-ray free-electron laser (XFEL) pulse's temporal structure through single- and double-crystal reflections of low and high orders. In addition to simulating the degree of smearing of an incident pulse's microbunching structure, the shot-to-shot time-integrated intensity fluctuations were examined (Fig. 1.5).

Attention has also been directed towards understanding the high-field-induced nonlinear corrections to the elastic-scattering cross section. This was deemed important in light of the possible necessity of modification of the electronic susceptibility for a dynamical diffraction theory valid at high x-ray intensities. Also motivating this issue is the frequently contemplated future technique of single-shot (or few-shot) diffraction studies of materials with focused XFEL beams. It is reasonable to ask whether, at such high intensities, the scattering intensities have the same quantitative interpretation (in connection to electronic structure) as in conventional x-ray scattering. To examine this, the next order perturbative correction to the usual (linear) scattering factor for x-rays was estimated to be 5 orders of magnitude weaker than the Thomson cross section.

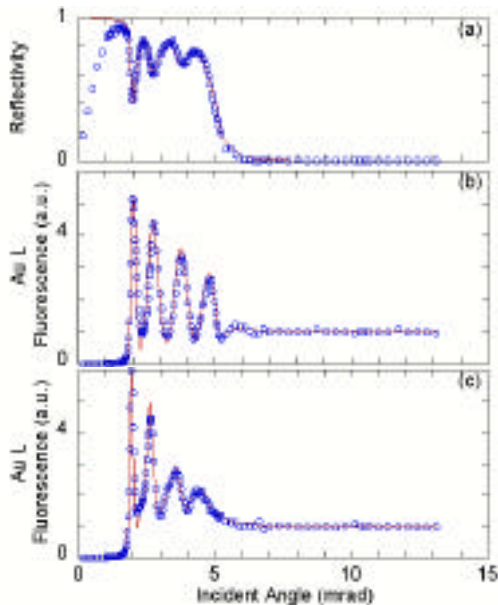


Fig. 1.4. Experimental data (circles) and fits (lines) at room temperature for (a) reflectivity and (b) fluorescence. The fluorescence profile after the sample has been annealed at 85°C for 180 minutes is shown in (c).

1.4 High-Energy X-ray Scattering

The high-energy x-ray program is heavily involved in the development of instrumentation and techniques that will be used on a dedicated high-energy beamline at the APS (the former HEX-CAT project).

Part of this effort is to develop the user base for high-energy x-rays from the existing community of x-ray and neutron users. High-energy x-rays are being used in a variety of scientific areas, but the largest use is now coming from applied materials science, in particular in the area of stress, strain, and texture measurements. The developments in high-energy small-angle scattering are unique and give a valuable new tool for examination of a variety of materials.

1.4.1 Development of a High-Energy SAXS Camera at Beamline 1-ID

High-energy small-angle x-ray scattering (SAXS) at second- and third-generation

synchrotron sources has been demonstrated (Siddons et al., 1990; Bosecke & Diet, 1997), based primarily on Bonse-Hart geometries. Our aim is to develop a high-energy (HE)-SAXS camera for beamline 1-ID based on an in-line geometry. The camera allows for collection of anisotropic SAXS information, with good spatial resolution and is compatible with other high-energy techniques under development at sector 1 (e.g., wide-angle x-ray scattering (WAXS) and phase-contrast imaging).

Unlike Bonse-Hart SAXS cameras, the in-line camera allows for fast data acquisition and makes possible time-resolved studies, as

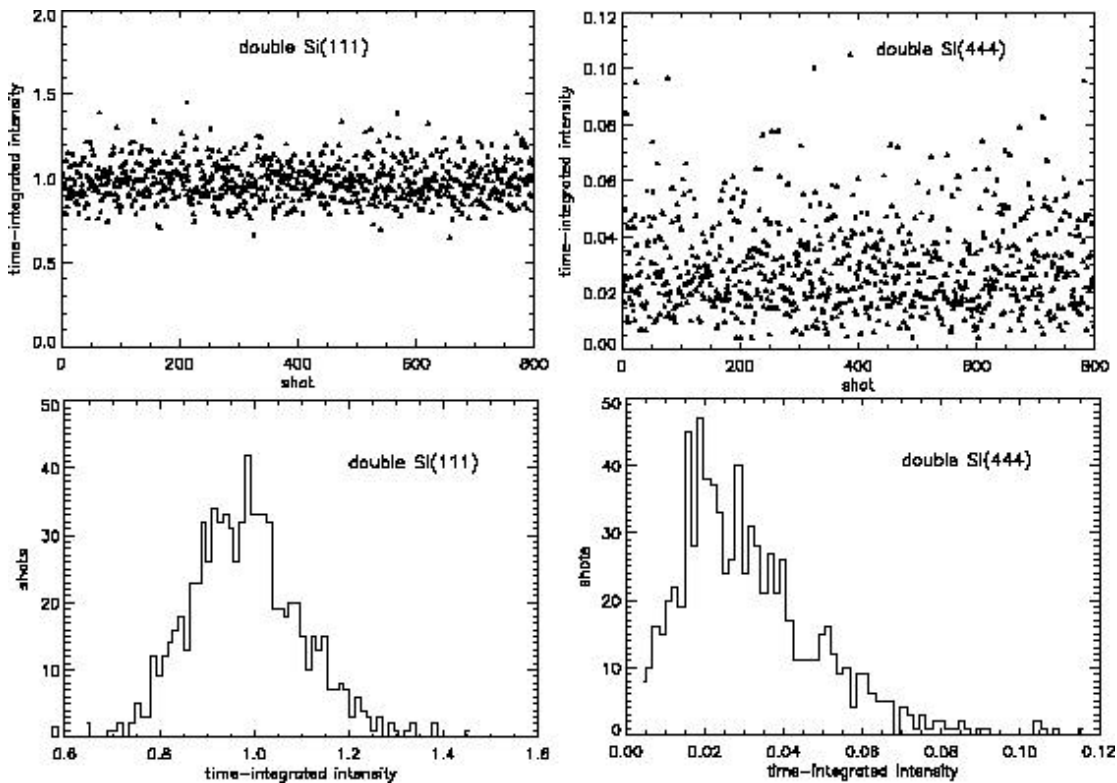


Fig. 1.5. Integrated intensity statistics of shot-to-shot fluctuations calculated after double Si(111) and Si(444) monochromators placed in an 8 keV SASE beam from the Linac Coherent Light Source (LCLS).

demonstrated for lower energy x-rays (Bras & Ryan, 1997).

Here we briefly outline instrumentation and data treatment and demonstrate the technique with spatially resolved measurements on thermal-barrier coatings grown by electron-beam phase vapor deposition (EB-PVD). This work was done in collaboration with a group from UNI-CAT/NIST. Many of the relevant properties of these coatings, including the elastic modulus and thermal conductivity, are related to the coating porosity and microcracking, which are in turn dependent on the deposition process parameters. Previous small-angle scattering (SAS) measurements on these coatings, using neutrons and lower energy x-rays (Allen et al., 2001) have revealed strong anisotropic SAS patterns related to orientation-dependent inhomogeneities. However since the beam size in those studies was on the order of the coating thickness ($\sim 800 \mu\text{m}$), no information on any gradients in the sample was obtained.

An 80.72 keV beam from the high-energy monochromator was reduced to $100 \times 20 \mu\text{m}^2$ using 2-mm-thick W slits. Additional guard slits were placed ~ 1 m downstream to minimize background arising from parasitic scattering. Direct beam intensity and sample transmission were monitored with an ion chamber and PIN diode placed just upstream and downstream of the sample position, respectively, and the incident flux was measured to be $\sim 3 \times 10^9$ ph/sec. The samples were cut into 0.5-mm-thick cross sections and measured in transmission geometry. The 2D SAXS intensity was recorded with a Bruker CCD detector located 4.9 m from the sample.

Figure 1.6 shows the sample transmission as a function of thickness. Within the coating, the transmission increases towards the top of

the coating due to an increase in porosity. Quantification of this porosity, by accounting for sample thickness and theoretical absorption factors, shows values ranging from 10-20% (Kulkarni et al., unpublished). Two-dimensional SAXS patterns are presented for four beam locations in Fig. 1.7. The SAXS patterns display marked anisotropies, as expected from the directional nature of deposition process and resulting porosity. Furthermore, differences in SAXS patterns are clearly visible as a function of position. Near the interface, the patterns show two maxima as a function of q , while, further up in the coating, additional maxima are present.

Complementary microscopy studies reveal that these SAXS patterns are caused by a hierarchy of nm-sized porosity formed during deposition. These range from inter-columnar pores near the interface (SEM image in Fig. 1.7) to oriented intracolumnar pores and feathery cracks (as seen by TEM, Kulkarni et al., unpublished) further up in the coating.

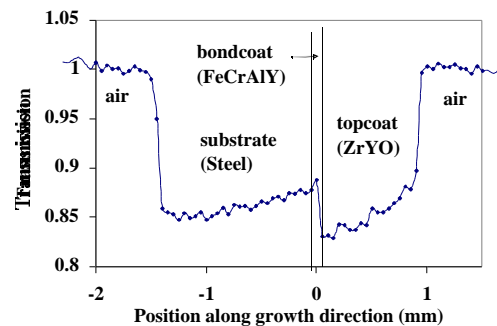


Fig. 1.6. Transmission across various layers of the thermal-barrier coating system. Spatial resolution ($25 \mu\text{m}$) is twice the spacing between points.

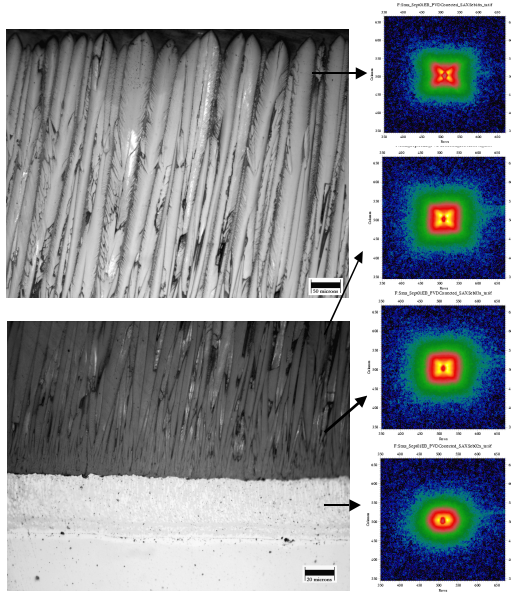


Fig. 1.7. Scanning electron microscope (SEM) images near the surface (top left) and interface (bottom left) of the TBC system, with corresponding HE-SAXS images (right).

1.4.2 Stress/Strain and Texture Measurements in Polycrystalline Materials

Most structural and functional materials are polycrystalline and understanding their bulk behavior is critical. Important structural parameters are the local stress/strain and texture. Applied materials are often heterogeneous with performance governed by structural gradients on the size of grains (often between 1-100 μm). To validate the various mesoscale models that are proposed, experimental data are necessary that are averaged over a statistical ensemble of grains but still resolve the macrogradients. Currently, such data are essentially nonexistent due to the lack of suitable experimental techniques.

High-energy x-rays are a powerful tool to gather such data. The combined penetration

power, ample flux, and small focal sizes (down to 1 μm) offer unique experimental capabilities. Furthermore, 2-D detectors provide parallel, and therefore fast, data acquisition, opening up opportunities with *in situ* measurements. Efforts of the SRI-CAT high-energy program are illustrated by the following example.

Fiber fracture in metal-matrix composites often initiates damage zones that grow until the composite fails. To better understand the evolution of such damage from a micromechanics point of view, a model Ti-matrix/SiC-fiber composite was studied. The transfer of load from a broken fiber to the rest of a fiber-reinforced composite is one of the fundamental micromechanical processes determining strength. In order to predict strength, one needs to understand the details of this load transfer.

Using high-energy x-rays and a small sampling volume, the damage zone around a broken fiber was investigated (in collaboration with a group from California Institute of Technology). The studied composite system consists of a single row of unidirectional SiC fibers (SCS-6, 140 μm diameter) in a Ti-6Al-4V matrix, prepared by a proprietary technique at 3M Corp. A small region of the matrix was removed via acid etching to expose the SiC fibers. One fiber was intentionally broken in the exposed region, with the matrix left intact around and behind the exposed region.

The strain in the fibers and matrix was monitored using a $90 \times 90 \mu\text{m}^2$ beam while applying a tensile stress to the sample. Results of the strains within the broken fibers are shown in Fig. 1.8. The data were compared to a modified shear lag model that considers the elastic response of the matrix and the fibers. A comparison of the model

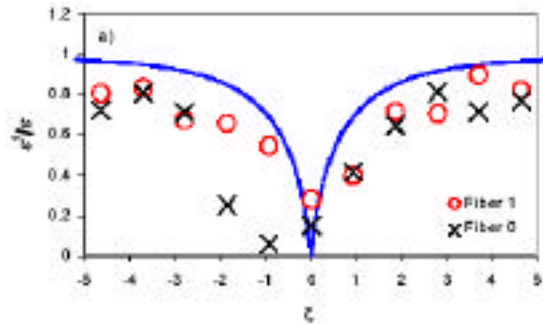


Fig. 1.8. Comparison of strains from model predictions (designated by lines) and XRD data from fibers (symbols). The applied stress was about 420 MPa. Strains were normalized with respect to the applied far field value. The dimensionless length describes the distance along the fibers from the crack.

and data shows a correlation on the trend of the data, but there are significant discrepancies. Results indicate the need for further refinements of the model, incorporating factors such as residual stress and matrix plasticity.

1.4.3 Resonant Powder Diffraction Studies of Gallium Distribution in the Type-I Clathrates

There has been considerable recent interest in the development of a new generation of more efficient materials for thermoelectric cooling. In order to achieve high efficiency, thermoelectric materials must simultaneously display reasonable electronic conductivity and very low thermal conductivity. The type-I clathrates $\text{Sr}_8\text{Ga}_{16}\text{Ge}_{30}$ and $\text{Sr}_4\text{Eu}_4\text{Ga}_{16}\text{Ge}_{30}$ display glass-like thermal conductivities along with relatively good charge carrier mobility making them good candidates for thermoelectric applications.

The static disorder associated with the presence of both gallium and germanium in

the framework has a significant effect on the electrical properties of these materials. In collaboration with a group from Georgia Institute of Technology and the University of South Florida, we used resonant powder diffraction to investigate the gallium distribution in the type-I clathrates $\text{Sr}_8\text{Ga}_{16}\text{Ge}_{30}$ and $\text{Sr}_4\text{Eu}_4\text{Ga}_{16}\text{Ge}_{30}$. The analysis indicates a pronounced preference for the occupation of the $6c$ site by gallium (Fig. 1.9).

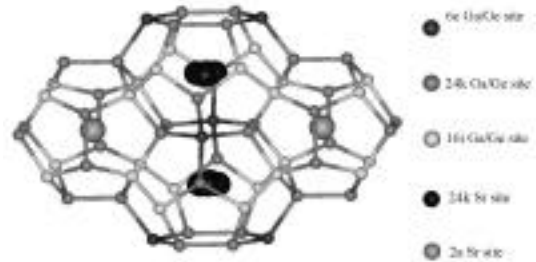


Fig. 1.9. Three crystallographically distinct sites exist in the framework of type-I clathrates, $6c$, $16i$, and $24k$. There is static disorder of gallium/germanium over these sites.

1.4.4 High-Energy X-ray Optics: Achieving Higher Energy Resolution with Compound Refractive Lenses and Crystals

A liquid-nitrogen-cooled monochromator for high-energy x-rays (50-300 keV) consisting of two bent Si(111) Laue crystals adjusted to sequential Rowland conditions (Fig. 1.10) has been in operation for over two years at the 1-ID beamline. It delivers over ten times more flux than does a flat crystal monochromator at high energies, without any increase in energy width ($\Delta E/E = 10^{-3}$). Cryogenic cooling permits optimal flux, avoiding a sacrifice from the often-employed alternative technique of white-beam filtration. The fixed offset geometry

provides a fully tunable, in-line mono-chromatic beam.

Although 10^{-3} energy resolution in the 50-100 keV range is sufficient for most high-energy experiments presently conducted at the 1-ID beamline (e.g., pair-distribution function measure-ments, fluorescence spectroscopy, powder diffraction, and stress/texture deter-mination), it is sometimes desirable to have a narrower energy bandpass. Improved energy resolution ($E/E = 10^{-4}$ or better) would benefit high-resolution powder diffraction, line-shape analysis in stress/strain measurements, anomalous scattering from heavy elements, excitation of nuclear resonances, Compton profile studies, and high-resolution spectroscopy for inner shell atomic physics.

One approach to narrowing the energy resolution to 10^{-4} levels or better is by maintaining the current concept but with modified Laue crystal parameters of thickness, asymmetry, and reflection order.

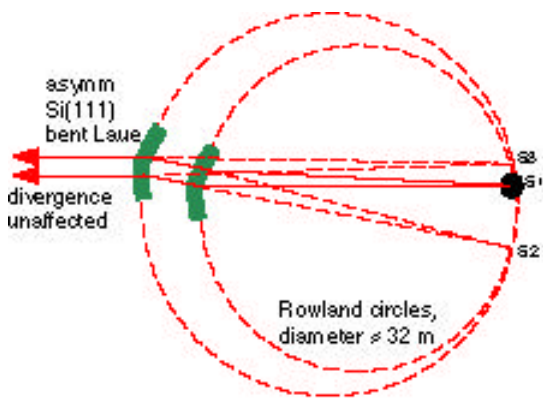


Fig. 1.10. Tunable, in-line high-energy x-ray monochromator composed of two vertically diffracting, bent Laue crystals located at about 32 m from the undulator source (S1).

However, higher resolutions at high x-ray energies demand excellent stability, which is difficult to achieve at the heat loads delivered by the white beam. So, attaining energy resolutions better than 10^{-4} is best done using additional postmono-chromatization optics after the existing broader bandwidth double-Laue system. This approach keeps the white beam optics invariant (and relatively simple), while permitting the subsequent high-resolution system to operate without significant thermal loads.

The post-monochromatization optics developed at 1-ID (Fig. 1.11) uses a compound refractive lens (CRL) to collimate (i.e., eliminate the angular divergence of) the beam from the double-Laue system. The resultant beam is better matched to the acceptance of the small angular width of the high-resolution, 4-reflection flat-crystal optics. The effectiveness of such a method is greatly enhanced by a pre-monochromator that is brilliance preserving—a feature inherent in the bent double-Laue system, but not, for example, in double mosaic-crystal monochromators, which are commonly used for high-energy x-rays. The performance of such an arrangement, as depicted in Fig. 1.11, is described here for an energy of 81 keV. The bent double-Laue pre-monochromator delivers 3×10^{12} ph/s in a 1×1 mm² beam of energy width $E/E = 1.5 \times 10^{-3}$ and a vertical divergence of 29 microrad. The beam then passes through an aluminum CRL consisting of 87 cylindrical holes of 1 mm diameter, separated by 50 micron walls. These parameters give the device a 35 m focal length for 81 keV radiation, resulting in the desired collimating action, as it is placed 35 m from the undulator source.

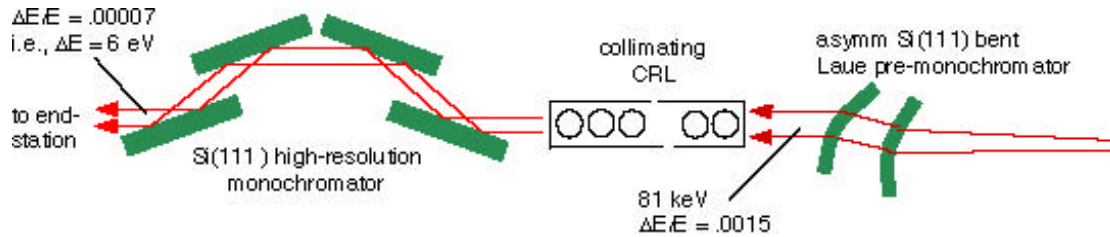


Fig. 1.11. High-resolution setup consisting of the bent Laue pre-monochromator, collimating lens, and 4-reflection flat crystal optics.

The collimated beam then Bragg reflects through four symmetric Si (111) crystals in a (+--+) configuration implemented by two dispersive channel-cut crystals. At 81 keV, a symmetric Si(111) Bragg crystal has energy and angular Darwin width acceptances of 1.4×10^{-4} and 3.5 microrad, respectively. So, ideally, one would expect this setup to monochromatize the beam to $E/E = 1.4 \times 10^{-4}$ with a flux loss (relative to the pre-monochromator output) of a factor of about 20. The flux loss is from a one order of magnitude improvement in monochromaticity with a 50% absorption loss through the CRL. In the experiment, a flux loss factor of about 50 was measured, a factor of 2 worse than expected. This is attributed to imperfect CRL collimation due to cylindrical aberrations. However, it turns out that this imperfect collimation also results in the final energy resolution being twice better than expected, i.e., 7×10^{-5} instead of 1.4×10^{-4} . So the final 81 keV beam intensity is 6×10^{10} ph/s in a 1×0.5 mm size (horiz. \times vert.), with 6 eV energy resolution.

To test focusing with CRLs at high energies, an aluminum CRL similar to the one described above, but with 212 holes, was used to vertically condense the 1×1 mm² beam from the bent Laue monochromator into the end station located 25 m beyond the CRL. This 1:0.7 distance ratio geometry

produced a 1.7×0.089 mm² (horiz \times vert) line focus with a CRL transmission of 27%. The 90 micron spot size is roughly twice that expected from the source size, with the discrepancy most likely again due to cylindrical aberrations in the CRL.

The elimination of cylindrical aberrations by using parabolic, as opposed to cylindrical, holes in the CRLs would improve performance in both the high-energy-resolution and focusing optics. A novel approach to fabricating one-dimensionally parabolic aluminum CRLs by an extrusion process is being developed and is described elsewhere in this report.

1.4.5 High-Energy X-ray Fluorescence: Minority Additives in Arc Lamp Plasmas

In principle, almost all elements can be identified by fluorescence lines below 25 keV, without the necessity for a very high energy incident x-ray beam. All K lines for the lighter elements and L lines for the heavier ones are available below this energy. However, detection of heavy elements by K-shell excitation can be attractive. The merits of the K-line fluorescence detection approach include (i) penetration capability of the radiation both entering and leaving a dense or contained sample, and (ii) simpler spectra, uncomplicated by the presence of

numerous overlapping peaks as often encountered when dealing with L-lines and standard solid-state detectors. K-holes also have higher radiative yields, but these advantages must be weighed against the backgrounds from strong Compton scattering processes (both simple and multiple) at high energies.

An example of the application of K-shell fluorescence spectroscopy is the study of minority additives in arc lamp plasmas.

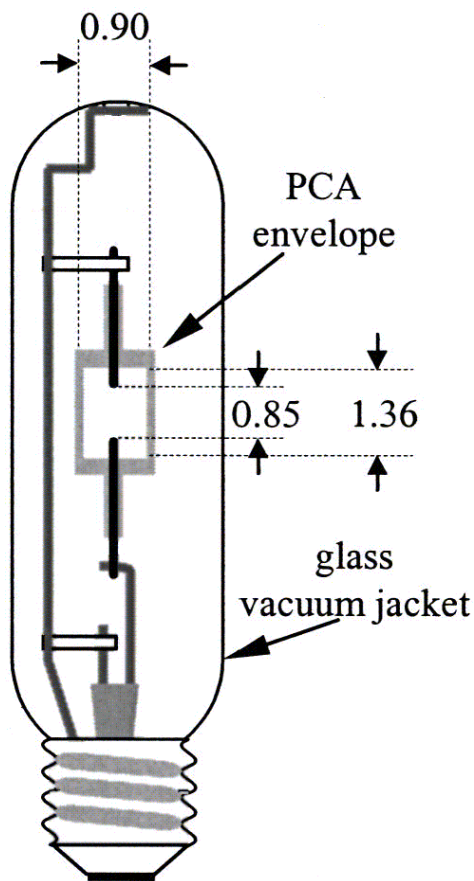


Fig. 1.12. The high-pressure arc lamp studied with x-ray-induced fluorescence consists of a ceramic alumina arc tube and a glass vacuum jacket. The arc tube is dosed with 16 mg Hg, 6.8 mg DyI₃, 1.2 mg CsI, and 12 Pa (90 Torr) Ar. (Dimensions are in mm.)

Small quantities of heavy-element additives (e.g., Dy, Ce, I) can significantly alter the lighting properties (spectral color and efficiency) of Hg lamps. The gas under arc-discharge is contained in jackets of ceramic alumina and pyrex, amounting to many millimeters of thickness for incident and fluorescence x-rays to penetrate (Fig. 1.12).

By using 60-90 keV incident radiation and detecting K-fluorescence, wall absorption does not pose a problem, and the spatial distribution of the minority additives relative to the majority species (Hg) can be measured (Fig. 1.13).

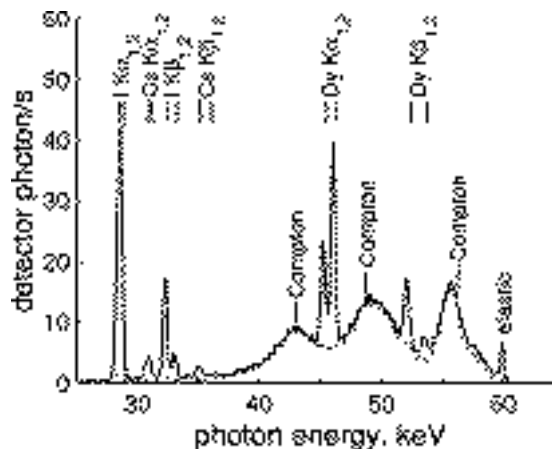


Fig. 1.13. X-ray-induced fluorescence spectrum of a 150 W ceramic metal-halide lamp with the lamp off (dotted line) and lamp on (solid line) showing characteristic fluorescence from Dy, I, and Cs, as well as Compton scattering from the lamp envelope, and elastic scattering from the envelope and Hg vapor.